Electronic Supplementary Material (ESI) for Physical Chemistry Chemical Physics.

Supplementary Information: Snowball formation for Cs^+ solvation in molecular hydrogen and deuterium

Josu Ortiz de Zárate,[†] Massimiliano Bartolomei,[†] Tomás González-Lezana,[†] José Campos-Martínez,[†] Marta I. Hernández,[*,†] Ricardo Pérez de Tudela,[‡] Javier Hernández-Rojas,[¶] José Bretón,[¶] Fernando Pirani,[§] Lorenz Kranabetter,[‖] Paul Martini,[‖] Martin Kuhn,[‖] Felix Laimer,[‖] and Paul Scheier[‖]

†*Instituto de Física Fundamental, Consejo Superior de Investigaciones Científicas (IFF-CSIC), Serrano 123, 28006 Madrid, Spain*

‡*Lehrstuhl für Theoretische Chemie, Ruhr-Universität Bochum, 44780 Bochum, Germany*

¶*Departamento de Física and IUdEA, Universidad de La Laguna, 38205, La Laguna, Tenerife, Spain*

§*Dipartimento di Chimica, Biologia e Biotecnologie, Università di Perugia, Perugia, Italy*

‖*Universität Innsbruck, Institut für Ionenphyisk und Angewandte Physik, Technikerstraße 25, 6020 Innsbruck, Austria*

E-mail: marta@iff.csic.es

Contents

1) Experimental Setup

The experiment utilizes helium nanodroplets as a matrix environment to facilitate the formation of cold ionic cluster complexes. Dopants are picked up from the gaseous phase by a helium nanodroplet beam, produced by free jet expansion of pressurized He (purity 99.9999%, Linde) through a cooled 5 μm nozzle. The temperature of the nozzle (9– 12 K), the stagnation pressure before the nozzle (20–25 bar) as well as the pressure in the vacuum vessel (10^{-4} mbar under operating conditions) determine the size distribution of the helium droplets.[1,2] The dopant is either already in gas phase or is evaporated in an oven and then exposed to the beam. Cesium (Sigma-Aldrich, purity 99.95%) was evaporated in an ohmically heated oven at a temperature of 328 K and hydrogen (purity 99.999%, Messer) or deuterium (purity 99.7%, Messer) were introduced afterwards in a differentially pumped region. Neutral cesium atoms or clusters are strongly heliophobic and occupy dimple sites at the surface of the He droplets,[3] even in the presence of a highly polarizable complex such as C_{60} inside the droplet,[4] whereas hydrogen molecules are heliophilic and submerge into the droplet.

After an atom or a molecule is picked up by a droplet, evaporative cooling boils off helium until a terminal temperature (0.4 K) is reached or no helium remains to be ejected. Excess energy released by the formation of molecular bonds or subsequent ionization processes can also be dissipated via the same mechanism. Ionic complexes tagged with some He atoms are expected to be at temperatures corresponding to the binding energy of the most weakly bound He atom.

Electron bombardment of the doped helium droplet can produce ionization of the alkali atoms by Penning ionization or ionization of hydrogen molecules via charge transfer from

He^+.[2] It is found that initial ionization of Cs is the dominant mechanism since $(H_2)_nCs^+$ clusters are observed at electron energies lower than 25 eV, the threshold for ionization of heliophilic dopants, and their abundance does not increase significantly for larger energies. Hence, formation of $(H_2)_nCs^+$ clusters (or $(D_2)_nCs^+$) mainly occurs in the interior of the droplet once the Cs^+ ion is formed at the surface and subsequently submerges into the droplet due to attractive electrostatic forces. As the initial He droplets contain $\sim 10^6$ atoms, the energy provided by the electron bombardment is insufficient to completely vaporize the droplet. It is rather expected that the droplet becomes multiply charged[5,6] and that the ions measured in the mass spectra are pushed out of the droplet by the presence of additional positively charged ions. Excess energy provided by these highly exothermic reactions lead to the evaporation of preferably weakly bound hydrogen molecules, which leads to the relative enhancement of the yield of particularly stable $(H_2/D_2)_nCs^+$ clusters.

Resulting mass spectra and ion efficiency curves are recorded with a high-resolution time of flight mass spectrometer.[7] The initial size distribution of the helium nanodroplets has to be optimized to match the chosen pickup conditions and ionization parameters. Mass spectra were evaluated by means of a custom-designed software.[8] The routine includes automatic fitting of a custom peak shape to the mass peaks and subtraction of background by fitting a spline to the background level of the raw data.

2) Potential Energy Surface (PES)

The total interaction potential for $(H_2)_nCs^+$ is assumed to be a sum of two-body (2B) and three-body (3B) interactions:

$$V\left[(H_2)_nCs^+\right] = \sum_{i=1}^{n} V^{2B}\left[H_2(i)\text{–}Cs^+\right] + \sum_{i<j}^{n} V^{2B}\left[H_2(i)\text{–}H_2(j)\right] + \sum_{i<j}^{n} V^{3B}\left[H_2(i)\text{–}Cs^+\text{–}H_2(j)\right]. \quad (1)$$

First, for the H_2-Cs^+ 2B interaction, we have developed a new H_2-Cs^+ PES optimized on accurate CCSD(T) interaction energies and obtained with the d-aug-cc-pV6Z[9] and def2-AQVZPP[10] basis sets for H_2 and Cs^+, respectively. We have checked that the adopted basis set is sufficiently large to guarantee well converged interaction energies, which are found to deviate from those carried out in the global minimum region with the d-aug-cc-pV5Z/def2-AQVZPP set of less than 0.9 meV (about 1%). The CCSD(T) computations have been performed using the Molpro2012.1 package.[11] The H_2 molecule has been assumed as rigid with an internuclear distance ρ= 0.766638 Å. The PES is then a function of only two Jacobi

coordinates: the modulus of the vector $\vec{r}$ between the center of mass of the diatomic and the cation, r, and the angle between $\vec{r}$ and the interatomic H_2 axis, θ. Four different angles were considered (shown in Fig.2 of the main article) The absolute minimum is found for the T-shaped configuration (θ=90^o), due to a leading charge-quadrupole interaction, with a well depth and equilibrium distance of 62.4 meV and 3.37 Å, respectively. The PES is quite anisotropic since for the linear geometry (θ=0^o) the well depth is reduced to 9.2 meV at a distance of 3.70 Å.

The H_2-Cs^+ 2B potential is represented analytically as a sum of non-covalent (V_{NC}) and electrostatic (V_{elec}) contributions. The electrostatic contribution entails intermolecular Coulomb interactions where Cs^+ is a monopole and a linear distribution of charges is adopted for H_2 (as in Ref.[12]), consisting of two charges placed on each of the nuclei and a third one, on the molecular center of mass. Those charges are derived from the molecule quadrupole moment using simple geometrical considerations. An accurate value of the H_2 quadrupole was estimated to be 0.48226 a.u. as a result of calculations at the multireference ACPF (Averaged Coupled Pair Functional) level with the aug-cc-pV6Z basis set[9] which were performed by following the guidelines reported in Ref.[13] In addition, the non-covalent term, V_{NC} , involving both induction and van der Waals interactions, is represented using the atom-bond model[14] and the Improved Lennard Jones (ILJ) formulation:[15]

$$V_{NC}(r,\theta) = \varepsilon(\theta)\left[\frac{m}{n(r,\theta)-m}\left(\frac{r_e(\theta)}{r}\right)^{n(r,\theta)} - \frac{n(r,\theta)}{n(r,\theta)-m}\left(\frac{r_e(\theta)}{r}\right)^{m}\right], \qquad (2)$$

where the long-range exponent m is set to 4 as corresponds to the leading charge-induced dipole force in $H_2 - Cs^+$ and

$$\begin{aligned} n(r,\theta) &= \beta + 4\left(\frac{r}{r_e(\theta)}\right)^2 \\ \varepsilon(\theta) &= \varepsilon^{\perp}\sin^2(\theta) + \varepsilon^{\parallel}\cos^2(\theta) \\ r_e(\theta) &= r_e^{\perp}\sin^2(\theta) + r_e^{\parallel}\cos^2(\theta). \end{aligned} \qquad (3)$$

Starting with an initial guess based on physical grounds (monomer polarizabilities[16–18]), parameters $\varepsilon^{\perp}$, $\varepsilon^{\parallel}$, $r_e^{\perp}$, $r_e^{\parallel}$ and β where fine-tuned by comparison with the CCSD(T) calculations. The analytical potential is compared with the CCSD(T) calculations in Fig.2 of the main article, where it can be seen that the agreement is excellent.

Regarding the second term in Eq.1, the H_2-H_2 2B potential, we have also adopted simple analytic expressions combining non-covalent and Coulomb-type contributions:

$$V^{2B}\left[H_2(i)-H_2(j)\right] = V_{NC}(r_{ij},\theta_i) + V_{NC}(r_{ij},\theta_j) + V_{elec}(r_{ij},\theta_i,\theta_j,\phi_{ij}), \qquad (4)$$

where diatom-diatom Jacobi coordinates are used, i.e., r_{ij} is the distance between the $H_2(i)$ and $H_2(j)$ centers of mass, θ_i and θ_j are the angles between the axes of $H_2(i)$ and $H_2(j)$ and the intermolecular direction, and ϕ_{ij} is the torsion angle. On the one hand, the electrostatic term V_{elec} is obtained using the same point charges representing the H_2 quadrupole, described above. On the other hand, the non-covalent contribution is given as a sum of two atom-bond potentials: the first one, $V_{NC}(r_{ij}, \theta_i)$, stands for the interaction between a rotating $H_2(i)$ molecule and $H_2(j)$, the latter treated as a pseudo-atom, whereas diatoms change roles for the second atom-bond interaction, $V_{NC}(r_{ij}, \theta_j)$. Both contributions are formally identical and given by an atom-bond ILJ function (Eq. 2). The corresponding parameters $\varepsilon^{\perp}$, $\varepsilon^{\parallel}$, $r_e^{\perp}$, $r_e^{\parallel}$ and β ($m = 6$ as corresponds to a pure van der Waals interaction) have been fitted to the accurate PES of Patkowski *et al*[19] which is based on high level *ab initio* calculations. We decided to use the simpler form of Eq.4 (as compared with the PES of Ref.[19]) for consistency in the complete force field model and for simplicity in the computation of first derivatives, needed for some of the theoretical methods. Present potential is compared with the Patkowski *et al* PES in Fig. S1, where it can be seen that the agreement is quite good.

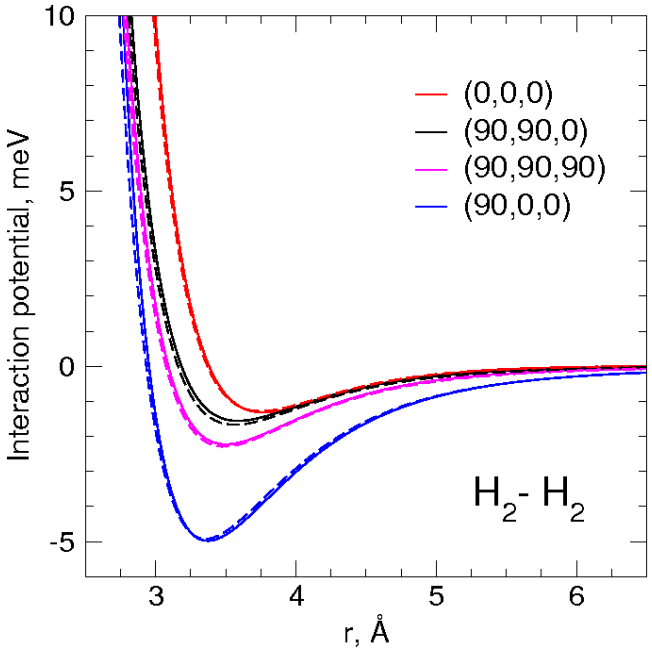

Figure S1: **H_2-H_2 interaction potential** (in meV) as a function of the intermolecular distance r (in Å) and for various relative orientations $(\theta_a, \theta_b, \phi_{ab})$= (0,0,0), linear; (90,90,0), H-shaped, (90,90,90), X-shaped, and (90,0,0), T-shaped. Solid lines correspond to the present potential, which are compared with the Patkowski *et al*[19] PES, in dashed lines.

In addition to the reported 2B potentials that explicitly depend on the orientation of the H_2 molecules (rigid rotor approximation), we have also considered these molecules as pseudoatoms using potentials that represent the interaction averaged over all their orientations

(pseudoatom approximation). These orientationally averaged potentials are also represented by atom-atom ILJ functions as that of Eq. 2 but with constant well depths and equilibrium positions, $\bar{\varepsilon}$ and $\bar{r}_e$ (the electrostatic contribution cancels out by the averaging). It was found that setting these parameters to their spherical average (i.e., $\bar{r}_e = (2r_e^{\perp} + r_e^{\parallel})/3$, etc.), the corresponding ILJ function reproduces extremely well the result of the numerical integration of the angular-dependent potential. It is worth noting that the orientationally averaged H_2-H_2 potential is quite similar to that of Silvera-Goldman[20] as well as the spherically averaged Diep and Johnson potential.[21]

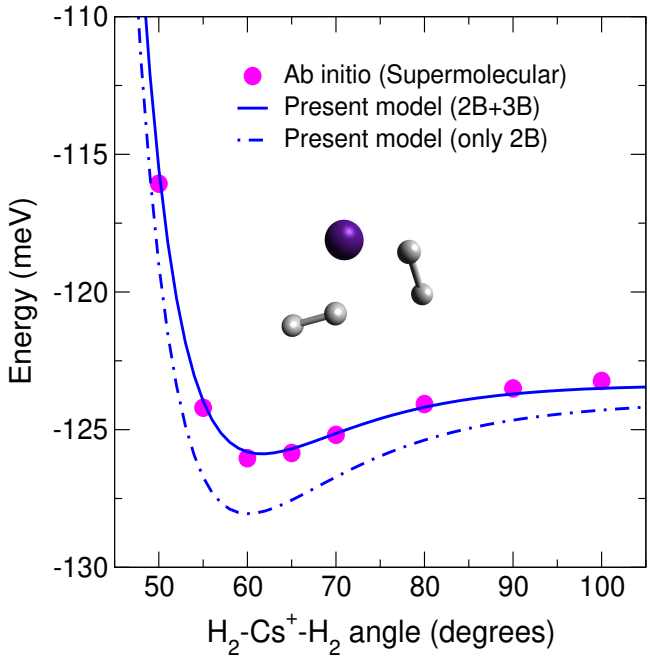

Figure S2: **$(H_2)_2$-Cs^+ interaction potential** (in meV) as a function of the angle formed between the vectors pointing to the centers of mass of the two H_2 molecules, with common origin at Cs^+. Throughout the scan, the H_2 molecular axes are perpendicular to these vectors (T-shaped configuration) as well as to each other. The distance between the H_2 molecules and Cs^+ is 3.374 Å. Filled pink circles: ab-initio CCSD(T) supermolecular calculations; solid (dashes-dotted) lines: present model (Eq.1), including (neglecting) the three-body terms. A good agreement with the *ab initio* energies is achieved, the 3B effects playing non-negligible role.

Finally, the third term in Eq.1 corresponds to the interaction between the dipoles that the cation induces in the hydrogen molecules i and j as employed in previous studies[22,23]

Table S1: Optimized parameters for the $(H_2)_n$-Cs^+ PES, within the rigid rotor and the pseudo-atom approximations. Distances $r_e^\perp$, $r_e^\parallel$, $\bar{r}_e$, and the internuclear H-H distance ρ are in Å, while well depths $\varepsilon^\perp$, $\varepsilon^\parallel$ and $\bar{\varepsilon}$ are in meV. Common for the two approximations are m and β (dimensionless) and α, the H_2 average polarizability (from Ref.[16]), in Å^3. H_2 partial charges are in units of the proton charge; q_H is located on top of the H nuclei and q_C at the bond center.

			Rigid rotor				Pseudo-atom	
Dimer	m	β	$r_e^\perp$	$r_e^\parallel$	$\varepsilon^\perp$	$\varepsilon^\parallel$	$\bar{r}_e$	$\bar{\varepsilon}$
H_2-Cs^+	4	8.0	3.43	3.47	37.09	51.75	3.44	41.98
H_2-H_2	6	7.0	3.46	3.50	1.30	2.00	3.47	3.07
α	0.7870							
ρ			0.76664					
H_2 charges			q_H =0.45955,		$q_C = -2q_H$			

$$
\begin{aligned}
V^{3B}\left[\mathrm{H_2}(i)\text{–}\mathrm{Cs^+}\text{–}\mathrm{H_2}(j)\right] \;=\; & -\frac{\alpha^2}{4}\left[3r_i g_3(r_j)g_5(r_{ij}) + 3r_j g_3(r_i)g_5(r_{ij})\right. \\
& -g_3(r_i)g_3(r_j)g_1(r_{ij}) - 6g_1(r_i)g_1(r_j)g_5(r_{ij}) \\
& \left.-2g_1(r_i)g_3(r_j)g_3(r_{ij}) - 2g_3(r_i)g_1(r_j)g_3(r_{ij})\right]
\end{aligned} \tag{5}
$$

where $g_n(r) = r^{-n}$, r_i and r_j are the distances between (the center of mass of) $H_2(i)$ and $H_2(j)$ to Cs^+, respectively, r_{ij} is the distance between the hydrogen molecules, and α is the polarizability of H_2. This magnitude is in fact a tensor which in the molecular frame is diagonal with two distinct components $\alpha_\parallel$ and $\alpha_\perp$, so in principle the polarizability varies with the orientation of the molecule with respect to the cation. We have found that this anisotropic contribution is negligible (less than 0.1 meV difference in the total energy as compared with using a spherically averaged polarizability, for $(H_2)_2Cs^+$ at equilibrium). Hence we have adopted, for the averaged polarizability, the reference value[16] $\alpha = 0.7870$ Å^3. The extent of these induction effects for the $(H_2)_2Cs^+$ cluster is shown in Fig.S2, where the interaction potential is studied as a function of the angle formed between the centers of mass of the two molecules, taking Cs^+ at the vertex. It can be seen that our potential model reaches a very good agreement with the *ab initio* (supermolecular) calculations of this cluster and for this, the contribution of the 3B terms is non-negligible.

We have checked that the inclusion in the interaction potential model of Axilrod-Teller-Muto long range term[22,24] has a negligible effect in the present system. Indeed, it has been found that, for the equilibrium structure of the n=3 cluster, the inclusion of this 3B dispersion contribution (taking the C_9 coefficient from Ref.[25]) provides a correction of 0.087 meV, which corresponds to about 0.05% of the total interaction energy, while that for the interacting induced dipole moments weighs for about 3%. This is because of the large size of the central ion which imposes large enough distances among the H_2 molecules so as to make this contribution very small. A similar conclusion was reached for the He_2Li^+ system.[22]

Optimized values of all the parameters involved in the analytical RigRot and PsAt PESs are given in Table S1.

3) Classical and Quantum Monte Carlo Methods

Energies and structures of the $(H_2/D_2)_nCs^+$ clusters were obtained using Basin-Hopping (BH), Path Integral Monte Carlo (PIMC) and diffusion Monte Carlo (DMC) methods, described below. On the one hand, the pseudoatom (PsAt) approximation and the corresponding PsAt PES were used for the first two methods. On the other hand, diffusion Monte Carlo calculations where performed considering the H_2/D_2 molecules as linear rigid rotors and using the more elaborated (RigRot) PES. Hydrogen and deuterium masses are m_H= 1.008 and m_D= 2.014 a.m.u. and the interatomic distance is 0.76664 Å.

3.a) Basin-Hopping

Within the PsAt approximation, putative global energy minima of $(H_2/D_2)_nCs^+$ clusters with $n \leq 30$ were located using the BH method[26] also known as the "Monte Carlo plus energy minimization" approach of Li and Scheraga.[27] This unbiased technique has been particularly successful for the global optimization of various atomic and molecular systems.[28–32] This technique is a stochastic method that involves perturbation followed by minimization each step. This method transform the PES into a collection of basins and explores them by hopping between local minima. Suitable parameters for the BH method were determined for all cluster sizes based on preliminary tests on $(H_2/D_2)_{13}Cs^+$. These benchmarks consisted of 10^4 minimization steps and were initiated from independent random geometries, varying the simulation temperature and the target acceptance ratios of the Monte Carlo simulation. Although our global minima remain putative, they were obtained in all trajectories. This should ensure a reasonably high degree of confidence.

The results were obtained at a constant simulation temperature of k_BT = 3 meV and

an acceptance ratio of 50%. A total of five runs of 2×10^5 basin-hopping steps each were performed for all sizes.

Quantum effects were included through calculation of the zero point energy (ZPE) in the harmonic approximation.[23,33,34] To do this we built a database of local minima close to the global minimum for each cluster size and choose the optimum BH+ZPE cluster geometry as that giving a minimum for the sum of the potential and the corresponding ZPE. In some cases, the geometry of this BH+ZPE global minimum differs from that of the BH one.

3.b) Path Integral Monte Carlo

The PIMC method has been reviewed extensively elsewhere.[35] In brief, static properties of a quantum system in thermodynamic equilibrium at temperature T can be accessed via the partition function, which can be computed as the trace of the density matrix operator. The thermal density of N quantum particles can be shown to be described by the density of N purely classical ring polymers, each having P beads. This is the so called classical isomorphism.[36] Neighboring beads within one polymer are connected by harmonic springs, whose force constants become weaker with increasing quantum character. Conversely, the quantum–classical isomorphism can be seen as having P replica of the system. Neighboring replica interact via the springs. Each replica is often regarded as *imaginary time slice*. Quantum mechanical effects such as delocalization or tunneling of the particles derive from the spread in position among the multiple beads that comprise the polymers. The price to pay in order to describe a quantum system by using a classical system is the appearance of multidimensional integrals. However, as the integrand is positive definite, Monte Carlo methods are most suited to perform these calculations.

The energy was computed following the thermodynamic estimator:[37]

$$\langle E(T) \rangle = \frac{3NP}{2\beta} - \left\langle \sum_{\nu=1}^{P} \sum_{i=1}^{N} \frac{1}{2} m_i \omega_i^2 (\mathbf{r}_i^{\nu} - \mathbf{r}_i^{\nu+1})^2 \right\rangle + \left\langle \frac{1}{P} \sum_{\nu=1}^{P} V(\mathbf{r}_1^{\nu} \dots \mathbf{r}_N^{\nu}) \right\rangle , \qquad (6)$$

where m_i is the mass of particle i and $\mathbf{r}_i^{\nu}$ describes the position of the bead ν of particle i. $\omega_i^2 = P/(\hbar\beta)^2$ is the frequency of the harmonic springs connecting the beads. Brackets indicate average over Monte Carlo steps, $\beta = (k_{\mathrm{B}}T)^{-1}$ and V is the PES.

In the present application, the $N = 1 + n$ particles correspond to the Cs^+ cation and to n H_2 (or D_2) molecules, treated within the PsAt approximation. Initial seeds are taken from the cluster optimized configurations obtained within the BH approach. Calculations were performed at 2 K, where still bosonic exchange is not expected to play any significant role. The ring polymers contained 500 beads, 16 of them were displaced at each Monte Carlo step according to the multilevel staging algorithm.[38,39] A total of 10^4 sweeps for thermalization

and 10^5 for statistics were performed, each sweep consisting of 10^3N MC steps. Standard deviations of the resulting cluster energies are obtained by the block average method.[40]

Various estimators were computed in order to get more insight into the structure of these clusters and the role of quantum effects. First, the degree of quantum delocalization of particle i is estimated by means of the radius of gyration:

$$RG_i = \sqrt{\frac{1}{P}\sum_{\nu=1}^{P}(\mathbf{r}_i^{\nu} - \mathbf{r}_i^{\mathrm{C}})^2} \tag{7}$$

where $\mathbf{r_i^C} = \mathbf{P^{-1}}\sum_{\nu=\mathbf{1}}^{\mathbf{P}}\mathbf{r_i^{\nu}}$ is the centroid of the polymer corresponding to particle i.

Moreover, the rigidity (solid-like versus liquid-like behavior) of the clusters is investigated by means of Lindemann index,[33,41] which for particle i expresses as:

$$\delta_i = \frac{1}{P(N-1)}\sum_{\nu=1}^{P}\sum_{j\neq i}^{N}\frac{\sqrt{\left\langle (r_{ij}^{\nu})^2\right\rangle - \left\langle r_{ij}^{\nu}\right\rangle^2}}{\left\langle r_{ij}^{\nu}\right\rangle} \tag{8}$$

where r_{ij}^{ν} is the distance between particles i and j at the time slice ν. A value of $\delta_i < 0.1$ indicates a quite rigid (solid) cluster, whereas a clear fluid behavior of the molecules corresponds to $\delta_i > 0.2$.[41]

Finally, in order to quantify the extent of the electrostriction effect on the H_2/D_2 molecules caused by the ionic impurity, the H_2-H_2 pair-distance distribution function was integrated for values of the distance below 3.06 Å. This distance corresponds to the point where the H_2-H_2 potential energy curve crosses the dissociation asymptote. The value of such integral gives a quantitative estimate of the percentage of the probability density that falls in the purely repulsive region of the H_2-H_2 interaction.

3.c) Diffusion Monte Carlo

The DMC method allows us the computation of the ground state of a system of quantum particles.[42–45] In this approach, the time-dependent Schrödinger equation transforms into a diffusion equation after changing the variable time, t, by imaginary time, $\tau = it$. Specifically, the diffusion equation for a system of N translating and rotating rigid bodies is

$$\hbar\frac{\partial\Psi}{\partial\tau} = -\left[\sum_{k=1}^{N} T_k^{trans} + T_k^{rot}\right]\Psi - V\Psi, \tag{9}$$

where T_k^{trans} and T_k^{rot} represent the translational and rotational operators for particle k and V is the potential energy operator. Its solution can be written as

$$\Psi(\tau) = \sum_l c_l \Phi_l e^{-\tau E_l/\hbar} \tag{10}$$

where Φ_l and E_l are the eigenstates and eigenenergies of the Hamiltonian. In this way, if the zero of energy is chosen such that all the eigenvalues are positive, the longest lasting term ($\tau \to \infty$) of Eq.10 will correspond to the ground state of the system.

The diffusion equation (Eq. 9) is solved by a random-walk method as follows. The function Ψ will be represented by population of replicas, each of them describing a specific position and orientation of all the particles of the system. At each time step $\Delta\tau$ the particles of each replica will randomly translate according to a Gaussian distribution depending on $\Delta\tau$ and the constants of the kinetic energy term (masses). Analogously, the rotational motion of the replicas is performed by randomly choosing a vector describing the angle and axis of rotation with a probability related to $\Delta\tau$ and the values of the moments of inertia of the rotor.[46] Finally, the potential term will determine the probability that a given replica will multiply or disappear. More details on the method are given elsewhere.[42–44]

In practice, we have used the code developed by Sandler and Buch[46,47] for the calculation of ground state energies and probability distributions of rotating H_2 (D_2) molecules attached to Cs^+. This technique has been successful in the study of various molecular clusters.[23,48,49] The (translational) motion of Cs^+ was explicitly described. For a typical cluster size ($n = 14$), six runs were usually performed, each of them involving- nine generations of a descendant weighting procedure.[44,50] An average of the final energies of the different runs is computed and an associated error bar is given by the standard deviation with respect to these runs. About 20000 replicas were propagated, first, using a time step of 20 a.u. for about 4000 steps. Then, in a second series, the time steps is enlarged to 80 a.u. and the propagation takes about 6000 steps. The initial population of replicas was built from a Gaussian spatial distribution (widths of about 0.3 Å) centered in a reference geometry corresponding to a putative minimum of the PES. This geometry was obtained by running classical Monte Carlo calculations with simulated annealing[51] and involving both translational and rotational moves. Several convergence tests were carried out by varying the parameters mentioned above and it was found that the resulting energies barely changed within the error bar associated to the reference calculation.

4) Additional Figures and Table

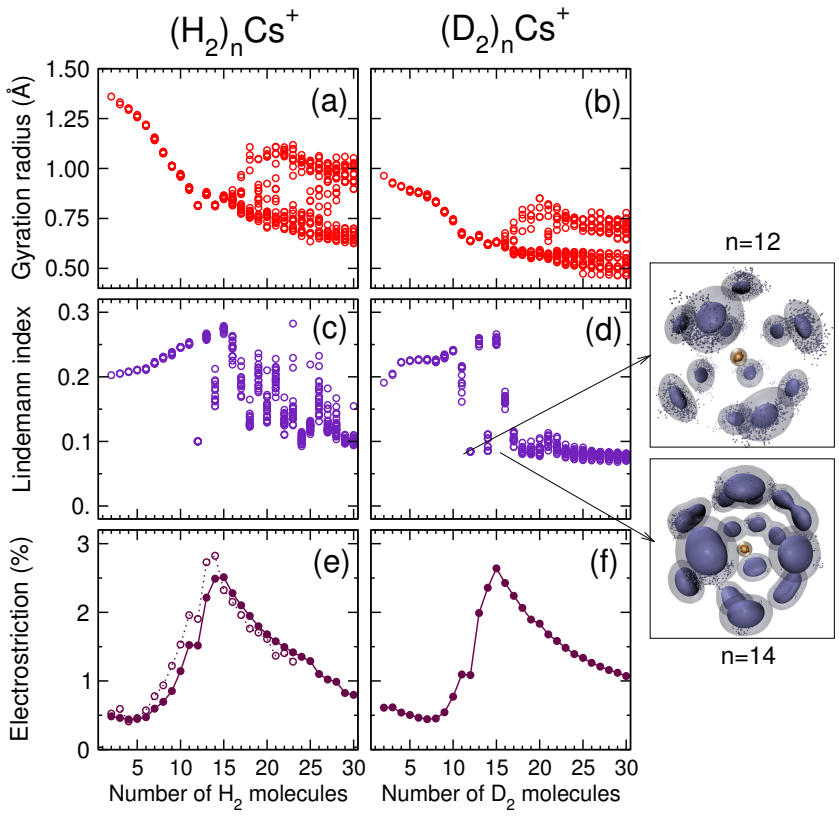

Figure S3: **Radius of Gyration (RG), Lindemann Index (LI) and Electrostriction of H_2/D_2 molecules, from PsAt PIMC calculations.** (a) and (b): RG (Eq.7) in Å. (c) and (d): LI (Eq.8). (e) and (f): Electrostriction (percentage of H_2-H_2 density in the repulsive region of H_2-H_2 potential), additionally computed within the RigRot (DMC) approach (dotted lines, empty circles). For $(H_2)_nCs^+$ (left panels), molecules are quite delocalized and fluid for $n < 12$ (large RG and LI). At $n = 12$ LI decreases indicating that the cluster becomes solid-like. For $n > 15$ there appear nearly two sets of values for the RG, associated to the inner and outer cluster shells. Electrostriction increases with n up to completion of the first solvation shell. For $(D_2)_nCs^+$ (right panels), RG are smaller (higher localization) as well as LI, particularly for $n = 14$ and $n > 16$, suggesting that deuterated clusters are solid-like for these sizes. Still, $(D_2)_{14}Cs^+$ is floppier than $(D_2)_{12}Cs^+$, as seen by the more dispersed LI values and the three-dimensional probability distributions shown on the right margin.

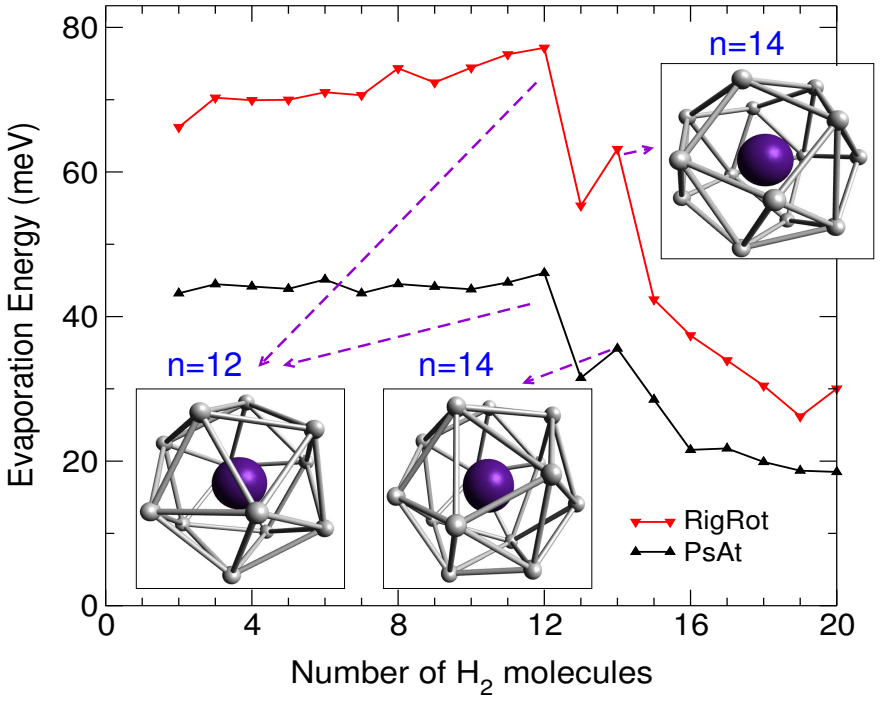

Figure S4: **Classical evaporation energies and structures of the most stable $(\mathbf{H_2})_n\mathbf{Cs^+}$ clusters:** Classical evaporation energies, $\Delta E_n = E_{n-1} - E_n$, where E_n refers to the minimum of the $(H_2)_nCs^+$ PES, within the rigid rotor (RigRot, in red) and the pseudoatom (PsAt, in black) approximations. The special stability of the n =12 and n =14 clusters is also clear at this level. Insets: Structures of the centers of mass of H_2 molecules. For n = 12 (lower-left inset), the H_2 molecules form an icosahedron with the cation at the center, this structure being the same within both approaches. The $(H_2)_{14}Cs^+$ cluster consists, within the PsAt approximation (lower-center inset), of 12 molecules forming two parallel hexagons, rotated 30^o one with respect to the other, the remaining two molecules being placed along the symmetry axis above and below the hexagons (D_{6d} symmetry, Kasper Z14 polyhedron[52]). Within the RigRot approach, this structure distorts to one of lower symmetry, where the six molecules forming the original hexagons do not reside in a common plane anymore (upper-right inset).

Table S2: Artificial modification of the V_{NC} component (Eq.2) of the H_2-Cs^+ interaction (remaining parameters from Table S1 unchanged). $r_e^{\perp,\parallel}$ and $\varepsilon^{\perp,\parallel}$ are balanced in order to keep the same long range behavior. Resulting equilibrium properties of the total H_2-Cs^+ PES are r_e and D_e (T-shape configuration).

	$r_e^{\perp}$ (Å)	$r_e^{\parallel}$ (Å)	$\varepsilon^{\perp}$ (meV)	$\varepsilon^{\parallel}$ (meV)	r_e (Å)	D_e (meV)
Modification 1	3.57	3.61	31.53	43.99	3.39	54.51
Modification 2	3.31	3.49	42.65	59.51	3.15	71.27

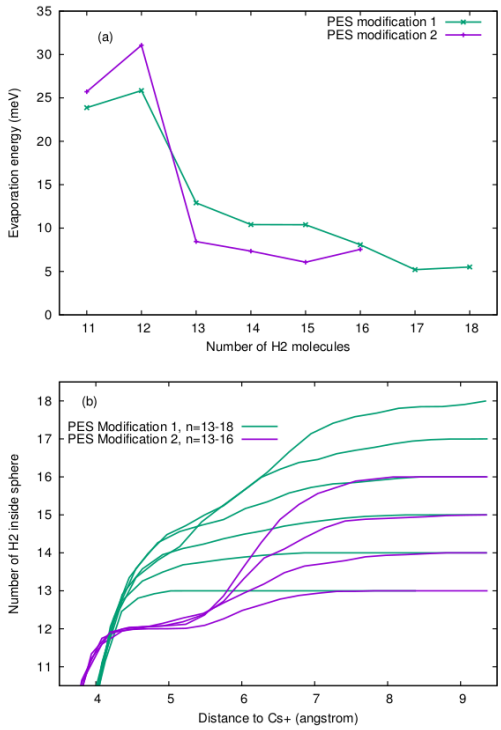

Figure S5: **Sensitivity of $(H_2)_nCs^+$ properties to variations of the H_2-Cs^+ potential (Table S2) with respect to the present PES (RigRot DMC calculations):** (a) As compared with Fig.1 of the main article, evaporation energies keep a clear maximum at n=12 but the peak at n =14 disappears; (b) As compared with Fig. 4 of the main article, Modification 2 leads to a distinct shell structure with 12 molecules in the first layer whereas for Modification 1 structures are more diffuse with a first layer containing 14-15 molecules.

References

(1) Gómez, L. F.; Loginov, E.; Sliter, R.; Vilesov, A. F. Sizes of Large He Droplets. *J. Chem. Phys.* **2011**, *135*, 154201.

(2) Mauracher, A.; Echt, O.; Ellis, A. M.; Yang, S.; Bohme, D. K.; Postler, J.; Kaiser, A.; Denifl, S.; Scheier, P. Cold Physics and Chemistry: Collisions, Ionization and Reactions Inside Helium Nanodroplets close to Zero K. *Phys. Rep.* **2018**, *751*, 1–90.

(3) Ancilotto, F.; Cheng, E.; Cole, M. W.; Toigo, F. The Binding of Alkali Atoms to the Surfaces of Liquid Helium and Hydrogen. *Z. Phys. B: Condens. Matter* **1995**, *98*, 323–329.

(4) Renzler, M.; Daxner, M.; Kranabetter, L.; Kaiser, A.; Hauser, A. W.; Ernst, W. E.; Lindinger, A.; Zillich, R.; Scheier, P.; Ellis, A. M. Communication: Dopant-Induced Solvation of Alkalis in Liquid Helium Nanodroplets. *J. Chem. Phys.* **2016**, *145*, 181101.

(5) Schöbel, H.; Bartl, P.; Leidlmair, C.; Daxner, M.; Zöttl, S.; Denifl, S.; Märk, T. D.; Scheier, P.; Spångberg, D.; Mauracher, A. et al. Sequential Penning Ionization: Harvesting Energy with Ions. *Phys. Rev. Lett.* **2010**, *105*, 243402.

(6) Mauracher, A.; Daxner, M.; Postler, J.; Huber, S.; Denifl, S.; Scheier, P.; Toennies, P. Detection of Negative Charge Carriers in Superfluid Helium Droplets: The Metastable Anions He^{*-} and He_2^{*-}. *J. Phys. Chem. Lett.* **2014**, *5*, 2444–2449.

(7) An der Lan, L.; Bartl, P.; Leidlmair, C.; Schöbel, H.; Jochum, R.; Denifl, S.; Märk, T. D.; Ellis, A. M.; Scheier, P. The Submersion of Sodium Clusters in Helium Nanodroplets: Identification of the Surface $\rightarrow$ Interior Transition. *J. Chem. Phys.* **2011**, *135*, 044309.

(8) Ralser, S.; Postler, J.; Harnisch, M.; Ellis, A. M.; Scheier, P. Extracting Cluster Distributions from Mass Spectra: Isotope Fit. *Int. J. Mass Spectrom.* **2015**, *379*, 194–199.

(9) Kendall, R. A.; Dunning, T. H.; Harrison, R. J. Electron Affinities of the First-Row Atoms revisited. Systematic Basis Sets and Wave Functions. *J. Chem. Phys.* **1992**, *96*, 6796.

(10) Weigend, F. Accurate Coulomb-Fitting Basis Sets for H to Rn. *Phys. Chem. Chem. Phys.* **2006**, *8*, 1057–1065.

(11) Werner, H.-J.; Knowles, P. J.; Lindh, R.; Manby, F. R.; Schütz, M.; Celani, P.; Korona, T.; Rauhut, G.; Amos, R. D.; Bernhardsson, A. et al. MOLPRO, Version2012.1, a Package of Ab Initio Programs. 2012; see http://www.molpro.net.

(12) Lombardi, A.; Pirani, F.; Laganà, A.; Bartolomei, M. Energy Transfer Dynamics and Kinetics of Elementary Processes (Promoted) by Gas-Phase CO_2-N_2 Collisions: Selectivity Control by the Anisotropy of the Interaction. *J. Comp. Chem.* **2016**, *37*, 1463–1475.

(13) Bartolomei, M.; Carmona-Novillo, E.; Hernández, M. I.; Campos-Martínez, J.; Hernández-Lamoneda, R. Long Range Interaction for Dimers of Atmospheric Interest: Dispersion, Induction and Electrostatic Contributions for O_2-O_2, N_2-N_2 and O_2-N_2. *J. Comp. Chem.* **2011**, *32*, 279–290.

(14) Pirani, F.; Albertí, M.; Castro, A.; Moix Teixidor, M.; Cappelletti, D. Atom-Bond Pairwise Additive Representation For Intermolecular Potential Energy Surfaces. *Chem. Phys. Lett.* **2004**, *394*, 37–44.

(15) Pirani, F.; Brizi, S.; Roncaratti, L.; Casavecchia, P.; Cappelletti, D.; Vecchiocattivi, F. Beyond the Lennard-Jones Model: a Simple and Accurate Potential Function Probed by High Resolution Scattering Data Useful for Molecular Dynamics Simulations. *Phys. Chem. Chem. Phys* **2008**, *10*, 5489–5503.

(16) Olney, T. N.; Cann, N. M.; Cooper, G.; Brion, C. E. Absolute Scale Determination for Photoabsorption Spectra and the Calculation of Molecular Properties Using Dipole Sum Rules. *Chem. Phys.* **1997**, *223*, 59–98.

(17) Hirschfelder, J. *Intermolecular Forces*; Wiley Interscience, 1967.

(18) Aquilanti, V.; Cappelletti, D.; Pirani, F. Range and Strength of Interatomic Forces: Dispersion and Induction Contributions to the Bonds of Dications and of Ionic Molecules. *Chem. Phys.* **1996**, *209*, 299–311, and references therein.

(19) Patkowski, K.; Cencek, W.; Jankowski, P.; Szalewicz, K.; Mehl, J.; Garberoglio, G.; Harvey, A. H. Potential Energy Surface for Interactions between Two Hydrogen Molecules. *J. Chem. Phys.* **2008**, *129*, 094304.

(20) Silvera, I. F.; Goldman, V. V. Isotropic Inter-Molecular Potential for H_2 and D_2 in Solid and Gas Phases. *J. Chem. Phys.* **1978**, *69*, 4209–4213.

(21) Diep, P.; Johnson, J. K. An Accurate H_2–H_2 Interaction Potential from First Principles. *J. Chem. Phys.* **2000**, *112*, 4465–4473, (Erratum: **2000**, *113*, 3480-3481).

(22) Liu, M. M.; Wu, M. S.; Han, H. L.; Shi, T. Y. Hyperspherical Coupled Channel Calculations of Energy and Structure of ^{4}He-^{4}He-Li^+ and its isotopic combination. *J. Chem. Phys.* **2016**, *145*, 034304.

(23) Rastogi, M.; Leidlmair, C.; An der Lan, L.; Ortiz de Zárate, J.; Pérez de Tudela, R.; Bartolomei, M.; Hernández, M. I.; Campos-Martínez, J.; González-Lezana, T.; Hernández-Rojas, J. et al. Lithium Ions Solvated in Helium. *Phys. Chem. Chem. Phys.* **2018**, *20*, 25569–25576.

(24) Prudente, F. V.; Marques, J. M. C.; Pereira, F. B. Solvation of Li^+ by Argon: How Important Are Three-Body Forces? *Phys. Chem. Chem. Phys.* **2017**, *19*, 25707–25716.

(25) Hinde, R. J. Vibrational Dependence of the H_2–H_2 C_6 Dispersion Coefficients. *J. Chem. Phys.* **2005**, *122*, 144304.

(26) Wales, D. J.; Doye, J. P. K. Global Optimization by Basin-Hopping and the Lowest Energy Structures of Lennard-Jones Clusters Containing up to 110 Atoms. *J. Phys. Chem. A* **1997**, *101*, 5111–5116.

(27) Li, Z. Q.; Scheraga, H. A. Monte-Carlo Minimization Approach to the Multiple-Minima problem in Protein Folding. *Proc. Natl. Acad. Sci.* **1987**, *84*, 6611–6615.

(28) Hernández-Rojas, J.; Bretón, J.; Gomez Llorente, J. M.; Wales, D. J. Lowest-Energy Structures of $(C_{60})_n$X(X=Li^+,Na^+,K^+,Cl^-) and $(C_{60})_n$YCl(Y=Li,Na,K) Clusters for $n \leq 13$. *J. Chem. Phys.* **2004**, *121*, 12315–12322.

(29) James, T.; Wales, D. J.; Hernández-Rojas, J. Global Minima for Water Clusters $(H_2O)_n, n \leq 21$, Described by a Five-Site Empirical Potential. *Chem. Phys. Lett.* **2005**, *415*, 302–307.

(30) Hernández-Rojas, J.; Bretón, J.; Gomez Llorente, J. M.; Wales, D. J. Global Potential Energy Minima of $C_{60}(H_2O)_n$ Clusters. *J. Phys. Chem. B* **2006**, *110*, 13357–13362.

(31) Hernández-Rojas, J.; Calvo, F.; Rabilloud, F.; Bretón, J.; Gomez Llorente, J. M. Modeling Water Clusters on Cationic Carbonaceous Seeds. *J. Phys. Chem. A* **2010**, *114*, 7267–7274.

(32) Hernández-Rojas, J.; Calvo, F.; Bretón, J.; Gomez Llorente, J. Confinement Effects on Water Clusters Inside Carbon Nanotubes. *J. Phys. Chem. C* **2012**, *116*, 17019–17028.

(33) Rodríguez-Cantano, R.; Pérez de Tudela, R.; Bartolomei, M.; Hernández, M. I.; Campos-Martínez, J.; González-Lezana, T.; Villarreal, P.; Hernández-Rojas, J.; Bretón, J. Coronene Molecules in Helium Clusters: Quantum and Classical Studies of Energies and Configurations. *J. Chem. Phys.* **2015**, *143*, 224306.

(34) Bartolomei, M.; Pérez de Tudela, R.; ; González-Lezana, T.; Hernández, M. I.; Campos-Martínez, J.; Villarreal, P.; Hernández-Rojas, J.; Bretón, J.; Pirani, F. Adsorption of Molecular Hydrogen on Coronene with a New Potential Energy Surface. *Phys. Chem. Chem. Phys.* **2017**, *19*, 26358.

(35) Ceperley, D. M. Path Integrals in the Theory of Condensed Helium. *Rev. Mod. Phys.* **1995**, *67*, 279.

(36) Chandler, D.; Wolynes, P. G. Exploiting the Isomorphism between Quantum Theory and Classical Statistical Mechanics of Polyatomic Fluids. *J. Chem. Phys.* **1981**, *74*, 4078–4095.

(37) Barker, J. A. A Quantum-Statistical Monte Carlo Method; Path Integrals with Boundary Conditions. *J. Chem. Phys.* **1979**, *70*, 2914–2918.

(38) Pollock, E. L.; Ceperley, D. M. Simulation of Quantum Many-Body Systems by Path-Integral Methods. *Phys. Rev. B* **1984**, *30*, 2555–2568.

(39) Sprik, M.; Klein, M. L.; Chandler, D. Staging: A Sampling Technique for the Monte Carlo Evaluation of Path Integrals. *Phys. Rev. B* **1985**, *31*, 4234–4244.

(40) Newman, M. E. J.; Barkema, G. T. *Monte Carlo Methods in Statistical Physics*; Oxford University Press, 1999.

(41) Calvo, F. Coating Polycyclic Aromatic Hydrocarbon Cations with Helium Clusters: Snowballs and Slush. *J. Phys. Chem. A* **2015**, *119*, 5959–5970.

(42) Anderson, J. B. A Random–Walk Simulation of the Schrödinger Equation: H_3^+. *J. Chem. Phys.* **1975**, *63*, 1499–1503.

(43) Anderson, J. B. Quantum Chemistry by Random-Walk - H ^2P, H_3^+ D_{3h} ^{1}A'$_1$, H_2 $^3\Sigma_u^+$, H_4 $^1\Sigma_g^+$, Be ^1S. *J. Chem. Phys.* **1976**, *65*, 4121–4127.

(44) Suhm, M. A.; Watts, R. O. Quantum Monte Carlo Studies of Vibrational States in Molecules and Clusters. *Phys. Rep.* **1991**, *204*, 293 – 329.

(45) McCoy, A. B. Diffusion Monte Carlo Approaches for Investigating the Structure and Vibrational Spectra of Fluxional Systems. *Int. Rev. Phys. Chem.* **2006**, *25*, 77–107.

(46) Buch, V. Treatment of Rigid Bodies by Diffusion Monte-Carlo. Application to the Para-H_2...H_2O and Ortho-H_2...H_2O Clusters. *J. Chem. Phys.* **1992**, *97*, 726–729.

(47) Sandler, P.; Buch, V. QCLUSTER code. **1999**,

(48) Gregory, J. K.; Clary, D. C. A Comparison of Conventional and Rigid-Body Diffusion Monte-Carlo Techniques: Application to Water Dimer. *Chem. Phys. Lett.* **1994**, *228*, 547–554.

(49) Kolmann, S. J.; D'Arcy, J. H.; Jordan, M. J. T. Quantum Effects and Anharmonicity in the H_2-Li^+-benzene complex: A Model for Hydrogen Storage Materials. *J. Chem. Phys.* **2013**, *139*.

(50) Kalos, M. H. Stochastic Wave Function for Atomic Helium. *J. Comp. Phys.* **1966**, *1*, 257 – 276.

(51) Wille, L. T. Minimum-Energy Configurations of Atomic Clusters: New Results Obtained by Simulated Annealing. *Chem. Phys. Lett.* **1987**, *133*, 405–410.

(52) Wales, D. J. *Energy Landscapes, with Applications to Clusters, Biomolecules and Glasses*; Cambridge University Press, 2003; p. 181.